

**Figure 1.** Lin28 and miRNA. (A) Architecture of the complex of Lin28 with miRNA.<sup>20</sup> (B) Alignment of pre-miR-363 sequences from several vertebrates. The conserved GGAG motif is highlighted (red box), and the region of the sequence corresponding to the miR-363<sup>19-46</sup> segment used in this study is colored orange; segments of full-length mature miR-363 are colored blue (5') and green (3'). (C) Schematic of Lin28 constructs used in this study. Secondary structures of (D) let-7g<sup>29-57</sup> and (E) miR-363<sup>19-46</sup>, predicted by MFOLD.<sup>27</sup>

strategy for producing stable, RNA-free, recombinant human Lin28. We show that the human protein binds both let-7g and miR-363 with high affinity in a 1:1 stoichiometry. We further show that this complex is resistant to changes in ionic strength. In contrast, the CSD on its own binds in a manner that is highly dependent on ionic strength. These data suggest that the electrostatic properties of CSD play a major role in helping Lin28 search for RNA targets in the transcriptome.

## EXPERIMENTAL PROCEDURES

**Protein Production.** The plasmid encoding the His-MBP-Lin28TT fusion protein (Figure 1C) was produced from the pETFF\_2 plasmid provided by the York Technology Facility. The sequence encoding residues 32–187 of human Lin28A (NCBI accession number NP\_078950.1) was amplified by polymerase chain reaction (PCR) from a synthetic, codon-optimized template (GeneArt). The pETFF\_2 vector was linearized by PCR and purified by agarose gel electrophoresis. The Lin28 sequence was then inserted into the pETFF\_2 vector using the In-Fusion ligation system (Clontech) and the product transformed into *Escherichia coli*.

The plasmid encoding the His-MBP-Lin28TT protein was transformed into the Rosetta2 (DE3) *E. coli* expression strain. Cells were grown in LB medium supplemented with 50  $\mu$ M ZnCl<sub>2</sub> to an OD<sub>600</sub> of 0.6. Expression was then induced by the addition of 1 mM isopropyl  $\beta$ -D-1-thiogalactopyranoside, and cells were grown overnight at 16 °C. Cells were harvested, resuspended on ice in 50 mM Tris-HCl (pH 7.5), 150 mM NaCl, 2 mM  $\beta$ -mercaptoethanol, 10  $\mu$ M ZnCl<sub>2</sub>, and 20 mM imidazole, and lysed by sonication. The lysate was applied to a Zn<sup>2+</sup>-charged 5 mL HisTrap column (GE Healthcare) at 4 °C. The column was then washed for 16 h (flow rate of 0.1 mL/

min) at 4 °C, with a solution containing 50 mM MES (pH 6.0), 1 M NaCl, 2 mM  $\beta$ -mercaptoethanol, 10  $\mu$ M ZnCl<sub>2</sub>, and 20 mM imidazole to remove nucleic acid contaminants. Bound proteins were eluted using 50 mM MES (pH 6.0), 1 M NaCl, 2 mM  $\beta$ -mercaptoethanol, 10  $\mu$ M ZnCl<sub>2</sub>, and 500 mM imidazole. The eluted protein was applied to a S200 10/300 gel filtration column (GE Healthcare) in a solution containing 10 mM MES (pH 6.0), 1 M NaCl, 2 mM  $\beta$ -mercaptoethanol, and 10  $\mu$ M ZnCl<sub>2</sub>. Fractions containing the Lin28 fusion protein were concentrated and dialyzed against a solution containing 10 mM Tris-HCl (pH 7.5), 150 mM NaCl, 2 mM  $\beta$ -mercaptoethanol, and 10  $\mu$ M ZnCl<sub>2</sub> before being flash-frozen in liquid nitrogen for storage.

**RNA Constructs.** Unlabeled and 5'-fluorescein-labeled RNA corresponding to human let-7g and miR-363 (Figure 1D,E) were synthesized by Dharmacon. A cytosine was introduced to the 5' end of the let-7g RNA for additional stability from base pairing. A similar approach was taken in previous studies of murine let-7g RNA.<sup>20</sup>

**SEC-MALLS.** A Biosep SEC S3000 column (Phenomenex) was pre-equilibrated with 20 mM Tris (pH 7.5) and 250 mM NaCl buffer and connected to a Dawn Helios II 18-angle light-scattering detector (Wyatt Technology). Lin28 fusion protein samples were diluted to 2 mg/mL (34 and 38  $\mu$ M for His-MBP-Lin28TT and His-MBP-CSD, respectively) in buffer or buffer with equimolar amounts of RNA oligonucleotide. The eluting species were detected by measuring the UV absorbance at 280 nm; the concentration of the species was determined using an Optilab rEX refractometer (Wyatt Technology), and a refractive index increment of 0.185 mL/g was used for calculation of the molecular weight in the ASTRA V software.

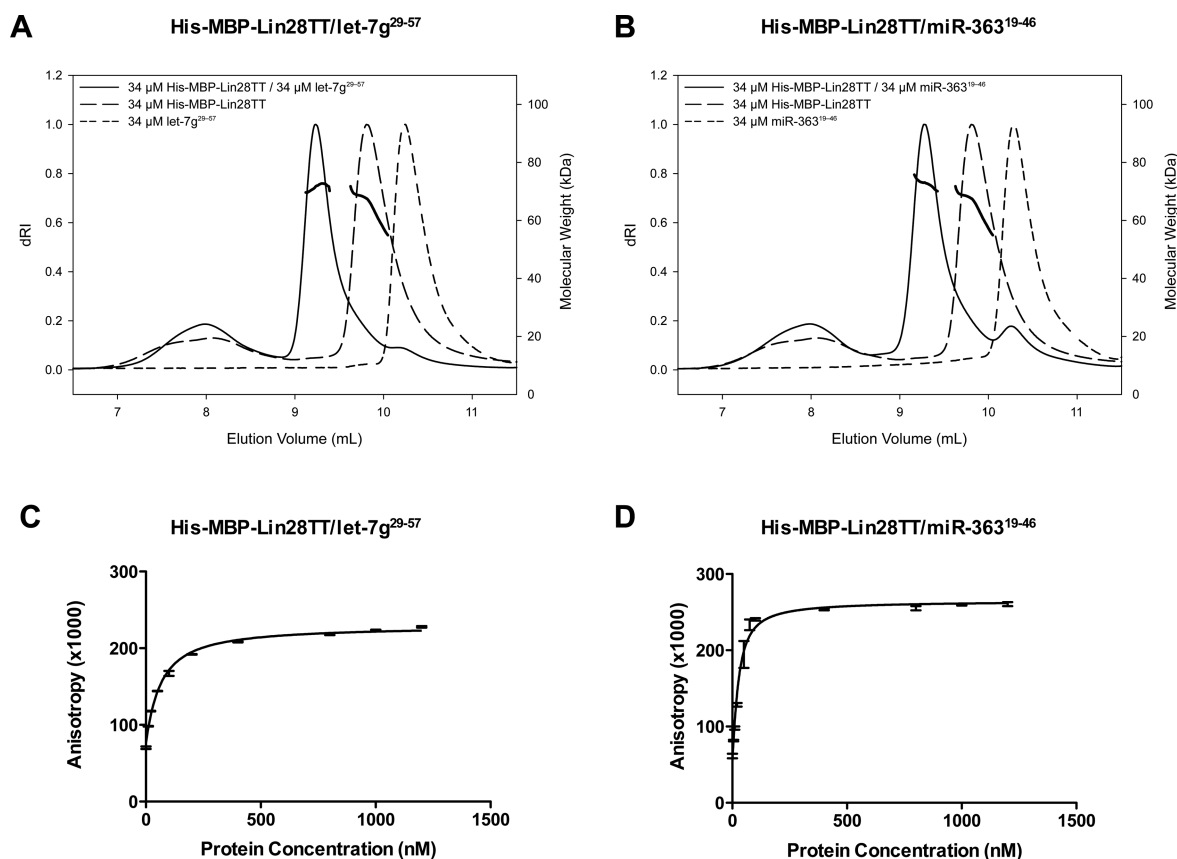


**Figure 2.** Analysis of the interaction of Lin28 with RNA. SEC–MALLS analysis of protein, RNA, and the protein–RNA complex with elution profiles shown for (A) let-7g<sup>29–57</sup> and (B) miR-363<sup>19–46</sup>. Fluorescence anisotropy analysis of the interaction of Lin28 with 5′-fluorescein-labeled (C) let-7g<sup>29–57</sup> and (D) miR-363<sup>19–46</sup> in 20 mM Tris-HCl (pH 7.5), 100 mM NaCl, 10 mM β-mercaptoethanol, 50 μM ZnCl<sub>2</sub>, and 0.01% (v/v) Tween 20.

Weight-average molecular weight values and the associated error of the fit are reported.

**Fluorescence Anisotropy.** Titrations were performed using increasing concentrations of protein and 20 nM 5′-fluorescein-labeled RNA in 200 μL final volumes, in triplicate. The sample buffer contained 20 mM Tris-HCl (pH 7.5), 50–750 mM NaCl, 10 mM β-mercaptoethanol, 50 μM ZnCl<sub>2</sub>, and 0.01% (v/v) Tween 20. Fluorescence readings were taken in a black flat-bottom 96-well plate (Nunc) at 25 °C in a BMG POLARstar Optima plate reader with the detector gain set using an initial measurement of 20 nM free fluorescein in buffer. Dissociation constants for His-MBP-Lin28TT–RNA interactions were determined by fitting the following equation in Prism (GraphPad):

$$y = A_{\min} + \frac{(A_{\max} - A_{\min})}{1 + \frac{c + x + K_d - \sqrt{(c + x + K_d)^2 - 4xc}}{2c}}$$

where  $x$  is the concentration of protein in nanomolar,  $y$  is the anisotropy (×1000),  $A_{\min}$  is the anisotropy of free labeled RNA,  $A_{\max}$  is the maximal anisotropy,  $c$  is the total concentration of labeled RNA (set to 20 nM), and  $K_d$  is the dissociation constant.

## RESULTS

**Human Lin28 Fused to MBP Can Be Purified as a Soluble, Nucleic Acid-Free Preparation.** Initial attempts to

produce nucleic acid-free human Lin28A as a His<sub>6</sub> fusion failed, as the protein quickly became lost upon removal of the nucleic acid with NaCl treatment (Figure S1). To improve solubility and stability, constructs were designed in which Lin28A (residues 32–187, Lin28TT) or the CSD on its own (residues 32–127) was fused with His-tagged maltose binding protein (His-MBP) via a three-alanine peptide linker (Figure 1C). A long salt wash was included in the purification protocol to remove nucleic acid contaminants, which otherwise caused all protein to elute as a high-molecular weight protein/nucleic acid mixture during size exclusion chromatography (Figure S2).

**Human Lin28 Forms 1:1 Complexes with let-7g and miR-363.** The His-MBP-Lin28TT fusion protein eluted in two steps during size exclusion chromatography: a sharp peak at 9.8 mL, corresponding to monomeric protein, with a weight-average molecular weight of  $65 \pm 4$  kDa, determined by MALLS (theoretical mass of 59.5 kDa), and a broad peak in the void volume, indicating aggregation and accounting for ~24% of the eluting protein mass, calculated on the basis of refractive index measurements.

Injecting equimolar amounts of His-MBP-Lin28TT and let-7g<sup>29–57</sup> RNA resulted in an earlier eluting peak relative to free monomeric protein and RNA (Figure 2A). An average molecular weight of  $72 \pm 1$  kDa was determined, comparable to the theoretical mass of 68.4 kDa for a 1:1 protein–RNA complex.

The interaction of Lin28 with miR-363 was investigated using a 28-nucleotide RNA segment, which includes the

characteristic stem loop and the conserved GGAG motif [miR-363<sup>19–46</sup> (Figure 1A,E)]. As with let-7g, an earlier eluting peak was observed for the protein/RNA mixture relative to free monomeric protein and RNA, with an observed molecular weight of  $73 \pm 2$  kDa (Figure 2B). This agrees with the 68.8 kDa mass calculated for a 1:1 protein–RNA complex.

#### Lin28 Binds let-7g and miR-363 with High Affinity.

The affinities of human Lin28 for let-7 RNA and miR-363 were subsequently measured. The fusion protein was titrated against a constant concentration of 5'-fluorescein-labeled let-7g<sup>29–57</sup> and miR-363<sup>19–46</sup>, and changes in fluorescence anisotropy were measured (Figure 2C,D). Equilibrium dissociation constants of  $54.1 \pm 4.2$  and  $16.6 \pm 1.9$  nM were deduced, respectively, under a 1:1 interaction model. No interaction was observed between the His-MBP tag and RNA (Figure S3). These data suggest that Lin28 binds let-7 RNA and miR-363 with comparable affinities.

**Lin28 CSD Forms Higher-Order Species with let-7g and miR-363 RNA.** To elucidate the role of the CSD in RNA binding, a His-MBP-CSD fusion protein was produced and its interactions with let-7g<sup>29–57</sup> and miR-363<sup>19–46</sup> were studied. A significant peak in the void volume during size exclusion chromatography indicated that His-MBP-CSD has a strong tendency to aggregate, with approximately 76% of the eluting protein present in this peak (Figure 3). A peak corresponding to the 52 kDa monomeric protein could still be observed, with an experimental molecular weight of  $52 \pm 1$  kDa. When the complex was mixed with let-7g and miR-363, a new peak corresponding to the complex was observed with average molecular weights of  $76 \pm 1$  and  $72 \pm 2$  kDa, respectively (Figure 3). These values are between the expected molecular weights of 62 and 113 kDa for 1:1 and 2:1 protein–RNA complexes, respectively. These data could be the result of protein aggregating while it is bound to RNA. Alternatively, they may indicate that the CSD does not bind RNA in a strict 1:1 manner, in agreement with previous reports on murine Lin28 forming high-order complexes with RNA.<sup>22</sup> In contrast with the relatively monodisperse 1:1 binding behavior exhibited by the full-length protein, it can be proposed that the ZnK domain facilitates the formation of stable 1:1 complexes.

**Lin28–miR363 Complexes Are Insensitive to Salt Concentration.** To determine if electrostatic forces play any role in the Lin28–miR-363<sup>19–46</sup> interaction, the fluorescence anisotropy experiments were repeated under different ionic strength conditions. As the exact nature of the His-MBP-CSD–RNA complexes is not known, an appropriate model for data fitting could not be determined. However, the general trend in the affinity of the interaction can be seen qualitatively by comparing the anisotropy at different ionic strengths. The data show that for the two-domain His-MBP-Lin28TT protein, the affinity of the interaction remained relatively constant under all conditions (Figure 4A and Table S1). Conversely, the His-MBP-CSD–miR-363<sup>19–46</sup> interaction became weaker as the ionic strength of the buffer increased (Figure 4B), so much so that no binding was observed at 750 mM NaCl. These data show that unlike the case for the two-domain protein, the interaction of the CSD with RNA is sensitive to ionic strength. This implies that electrostatic interactions have a far greater role when the ZnK domain is not present.

## DISCUSSION

**Lin28 Interacts with miR-363.** The miR-363 miRNA was identified as a potential binding partner of Lin28, as the 3'-

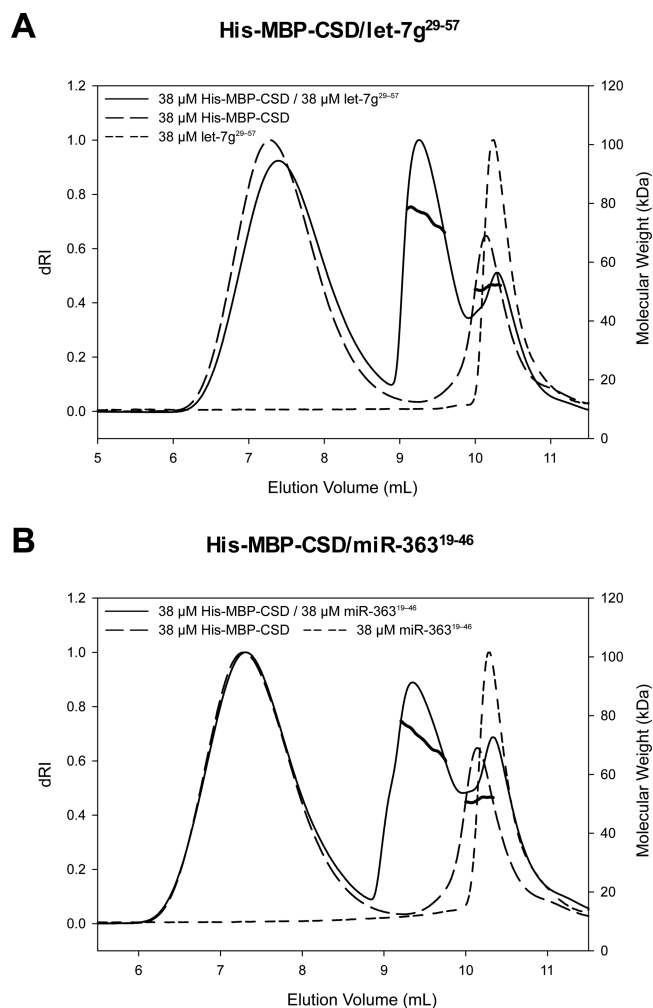


**Figure 3.** SEC–MALLS analysis of the interaction of His-MBP-CSD with RNA. Elution profiles are shown for protein, RNA, and protein–RNA complexes for (A) let-7g<sup>29–57</sup> and (B) miR-363<sup>19–46</sup>.

GGAG motif present in this sequence is highly conserved in land-based vertebrates. miR-363 is a member of the 106–363 miRNA cluster, a cluster paralogous to the 17–92 miRNA oncomir cluster.<sup>28,29</sup> Recent reports have identified miR-363 as a putative tumor suppressor. In neuroblastoma cells, miR-363 expression inhibits colony formation, growth, invasion, and metastasis through downregulation of the MYO1D and ADAM15 oncogenes.<sup>30</sup> miR-363 expression has been also linked with better prognosis and decreased metastatic potential in head and neck squamous cell carcinoma due to its targeting of podoplanin.<sup>31</sup> Expression of miR-363 also inhibits the growth of a cell line derived from a NK-cell lymphoma.<sup>32</sup> Given that both Lin28 and miR-363 are both implicated in the development of cancer, understanding the nature of Lin28–miR-363 interaction is of potential medical interest.

Previously reported  $K_d$  values for the interaction between Lin28 proteins and let-7 RNAs<sup>20–23,25,26</sup> display a large degree of variation, with differences of >4 orders of magnitude. The reasons for such a large discrepancy are likely complex and could range from sample preparation to buffer conditions to the length and structure of the oligonucleotide tested.

Here, we show that the miR-363 RNA segment containing the characteristic stem loop followed by the GGAG motif forms a relatively stable complex with a human Lin28A fusion protein,

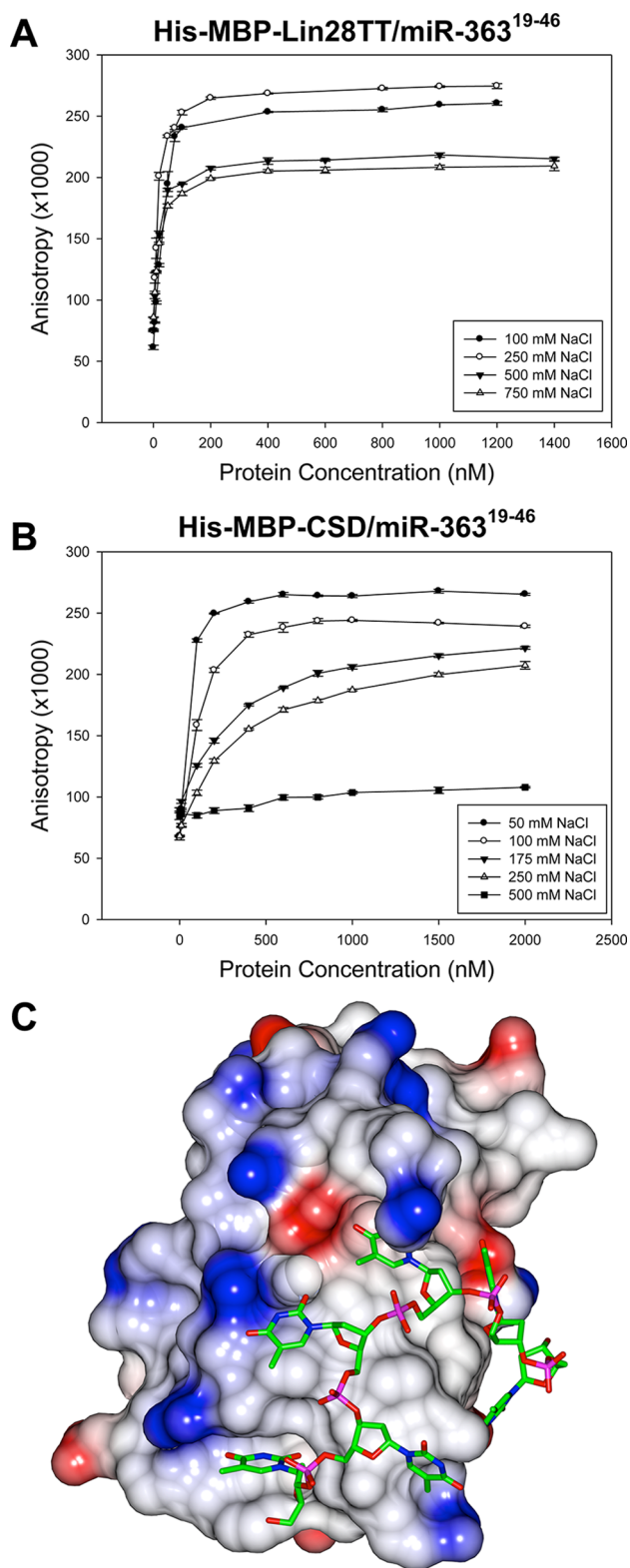


**Figure 4.** Effect of ionic strength on the interaction of Lin28 with miR-363. Fluorescence anisotropy experiments were conducted using fluorescein-labeled miR-363<sup>19-46</sup> at different ionic strengths with increasing concentrations of (A) His-MBP-Lin28TT or (B) His-MBP-CSD. (C) Model of the complex of human CSD with nucleic acid based on atomic structures of human Lin28b CSD (Protein Data Bank entry 4A4I) and the *Xenopus* Lin28b CSD–DNA complex (Protein Data Bank entry 4A75). The electrostatic surface potential for the human CSD, from  $-1$  V (red) to  $+1$  V (blue).

with a  $K_d$  of  $16.6 \pm 1.9$  nM under the described conditions (Figure 2D). SEC–MALLS analysis indicates a 1:1 protein:RNA stoichiometry in the complex (Figure 2B). We also observe a 1:1 interaction with an equivalent segment of let-7g RNA (Figure 2A), in agreement with an earlier observation of a 1:1 complex made with an RNA oligonucleotide of similar length and secondary structure, derived from the terminal loop of *Mmulet-7d*.<sup>20</sup> Additionally, the  $K_d$  of  $54.1 \pm 4.2$  nM of this interaction is comparable to the affinity of His-MBP-Lin28TT for the miR-363 RNA segment (Figure 2D). The data therefore indicate that Lin28 binds miR-363 and let-7 miRNAs in a similar manner.

This finding is of interest as the Lin28–miR-363 complex was shown to promote very little uridylation by Zcchc11 compared to that by let-7a-1.<sup>6</sup> In addition, the evidence of a direct interaction between amphibian Lin28 and miR-363, as well as the observation that knockdown of Lin28 results in decreased mature miR-363 levels, implies the alternative function of Lin28 as a positive regulator of miRNA biogenesis.<sup>24</sup> The results presented here show the similarities between the binding modes of let-7g and miR-363. Previously, it has been proposed that a change in the conformation of the 3' terminus of the let-7g hairpin caused by Lin28 binding may facilitate the recruitment of the TUTase responsible for let-7g uridylation.<sup>20</sup> Differences in the conformations of bound miR-363 and let-7g would not be detectable by the methods employed here but could account for the differences in the biological outcomes of Lin28 binding through the recruitment of different downstream effectors. Further studies identifying factors that may interact with and influence binding of Lin28 to miRNA, as well as structural information about such assemblies, may be useful for improving our understanding of this system.

**Determinants of Lin28:RNA Stoichiometry.** A recent study demonstrated that Lin28 binds the let-7g 46-nucleotide stem loop segment in a stepwise manner, with up to three protein molecules per RNA.<sup>22</sup> Interactions were mediated by three RNA segments, containing an exposed loop of the let-7g stem loop or either the 5'-GGAG-3' motif or its reverse (5'-GAGG-3'). The let-7g<sup>29-57</sup> oligonucleotide used here is shorter (29 nucleotides) and contains only the 3'-GGAG motif. Likewise, the miR-363<sup>19-46</sup> and *Mmu-let-7d* RNA oligonucleotides contain only one GGAG motif, at the 3' end. It is therefore possible that the stoichiometry of a Lin28–RNA complex is determined by (1) the number of GGAG motifs present in the RNA, which determine the specific attachment to RNA, and (2) the length of the RNA, which determines the number of CSD molecules that can be accommodated on exposed single-stranded RNA regions.

**Lin28 CSD Guides RNA Binding via Electrostatic Attraction.** The structures of murine Lin28A in complex with let-7 family miRNA sequences,<sup>20</sup> and of the *Xenopus* Lin28B CSD domain,<sup>21</sup> show binding of the CSD to single-stranded oligonucleotides through stacking interactions between the RNA bases and aromatic side chains on the CSD surface. In tandem, the ZnK domain binds the GGAG motif through a hydrogen-bonding network, with a stacking interaction formed between the side chain of Y140 and the bases of the final A and G of the motif.<sup>20</sup>

The sensitivity of the interaction of His-MBP-CSD with RNA to ionic strength (Figure 4B) implies that electrostatic forces play an equally important role in RNA binding. Examination of the CSD's electrostatic surface reveals clear areas of positive charge surrounding the nucleic acid binding

site (Figure 4C). Apart from Lys95 (Lys92 in the human CSD), the phosphate groups seen in the structure are not directly contacted by these areas of positive charge. However, a major difference between the bacterial cold shock protein homologues and the Lin28 CSD is the addition of two extra lysine residues to strand  $\beta$ 4, which results in a more basic binding platform.<sup>21</sup> It is therefore possible that these areas of positive charge could fulfill a key role in attracting and guiding RNA to the binding site, facilitating the formation of base-specific hydrophobic and hydrogen-bond interactions as observed in crystal structures.

In conclusion, we propose that Lin28 uses its CSD to sample the transcriptome through transient electrostatic associations, similar to how DNA binding proteins locate their target sites through facilitated diffusion, by “sliding” and “hopping”.<sup>33–36</sup> If Lin28 were to display a similar behavior, it would increase the likelihood of ZnK binding to the short GGAG motif for stable complex formation. Depending on the structure and sequence of the RNA, melting and the association of further Lin28 molecules could then occur. Such a model may also be relevant in light of recent work showing Lin28 can also bind to DNA and influence gene expression through the recruitment of epigenetic modification factors.<sup>37</sup> Future work will therefore need to elucidate Lin28's interaction with both the genome and transcriptome.

## ■ ASSOCIATED CONTENT

### ■ Supporting Information

The Supporting Information is available free of charge on the ACS Publications website at DOI: 10.1021/acs.biochem.6b00682.

Protein stability following removal of the nucleic acid via salt treatment (Figure S1), purification of His-MBP-Lin28TT (Figure S2), fluorescence anisotropy analysis of His-MBP with RNA (Figure S3), and equilibrium dissociation constants of the His-MBP-Lin28TT–miR-363<sup>19–46</sup> interaction at different NaCl concentrations, as measured by fluorescence anisotropy (Table S1) (PDF)

## ■ AUTHOR INFORMATION

### Corresponding Author

\*E-mail: fred.antson@york.ac.uk. Telephone: (44) 1904 328255.

### Present Addresses

<sup>§</sup>D.T.P.: Institute of Cell and Molecular Biosciences, Medical School, Cookson Building, Framlington Place, Newcastle University, Newcastle upon Tyne NE2 4HH, United Kingdom.

<sup>||</sup>F.C.W.: CRUK Beatson Institute, Garscube Estate, Switchback Road, Glasgow G61 1BD, United Kingdom.

<sup>⊥</sup>O.K.: Structural Studies Division, MRC Laboratory of Molecular Biology, Francis Crick Avenue, Cambridge CB2 0QH, United Kingdom.

### Funding

This work was supported by the Wellcome Trust (WT098230). D.T.P. was funded by a Ph.D. studentship from Yorkshire Cancer Research, and H.K.H.F. is supported by a Ph.D. studentship from the Wellcome Trust (WT095024MA).

### Notes

The authors declare no competing financial interest.

## ■ ACKNOWLEDGMENTS

We thank Christoph Baumann for useful suggestions, Andrew Leech for help in conducting experiments, and Phil Roberts for help in preparing Figure 1A.

## ■ ABBREVIATIONS

CSD, cold shock domain; ZnK, zinc knuckle; miRNA, microRNA; *Xenopus*, *Xenopus tropicalis*; *Mmu*, *Mus musculus*; MBP, maltose binding protein; His-MBP-Lin28TT, His-MBP-Lin28 with truncated termini; SEC–MALLS, size exclusion chromatography coupled with multiangle laser light scattering.

## ■ REFERENCES

- (1) Huang, Y. (2012) A mirror of two faces: Lin28 as a master regulator of both miRNA and mRNA. *Wiley Interdiscip. Rev. RNA* 3, 483–494.
- (2) Cho, J., Chang, H., Kwon, S. C., Kim, B., Kim, Y., Choe, J., Ha, M., Kim, Y. K., and Kim, V. N. (2012) LIN28A is a suppressor of ER-associated translation in embryonic stem cells. *Cell* 151, 765–777.
- (3) Hafner, M., Max, K. E. A., Bandaru, P., Morozov, P., Gerstberger, S., Brown, M., Molina, H., and Tuschl, T. (2013) Identification of mRNAs bound and regulated by human LIN28 proteins and molecular requirements for RNA recognition. *RNA* 19, 613–626.
- (4) Wilbert, M. L., Huelga, S. C., Kapeli, K., Stark, T. J., Liang, T. Y., Chen, S. X., Yan, B. Y., Nathanson, J. L., Hutt, K. R., Lovci, M. T., Kazan, H., Vu, A. Q., Massire, K. B., Morris, Q., Hoon, S., and Yeo, G. W. (2012) LIN28 binds messenger RNAs at GGAGA motifs and regulates splicing factor abundance. *Mol. Cell* 48, 195–206.
- (5) Mayr, F., and Heinemann, U. (2013) Mechanisms of Lin28-mediated miRNA and mRNA regulation—a structural and functional perspective. *Int. J. Mol. Sci.* 14, 16532–16553.
- (6) Heo, I., Joo, C., Kim, Y.-K., Ha, M., Yoon, M.-J., Cho, J., Yeom, K.-H., Han, J., and Kim, V. N. (2009) TUT4 in concert with Lin28 suppresses microRNA biogenesis through pre-microRNA uridylation. *Cell* 138, 696–708.
- (7) Yu, J., Vodnyanik, M. A., Smuga-Otto, K., Antosiewicz-Bourget, J., Frane, J. L., Tian, S., Nie, J., Jonsdottir, G. A., Ruotti, V., Stewart, R., Slukvin, I. I., and Thomson, J. A. (2007) Induced pluripotent stem cell lines derived from human somatic cells. *Science* 318, 1917–1920.
- (8) Hanna, J., Saha, K., Pando, B., van Zon, J., Lengner, C. J., Creighton, M. P., van Oudenaarden, A., and Jaenisch, R. (2009) Direct cell reprogramming is a stochastic process amenable to acceleration. *Nature* 462, 595–601.
- (9) Peng, S., Chen, L.-L., Lei, X.-X., Yang, L., Lin, H., Carmichael, G. G., and Huang, Y. (2011) Genome-wide studies reveal that Lin28 enhances the translation of genes important for growth and survival of human embryonic stem cells. *Stem Cells* 29, 496–504.
- (10) Yokoyama, S., Hashimoto, M., Shimizu, H., Ueno-Kudoh, H., Uchibe, K., Kimura, I., and Asahara, H. (2008) Dynamic gene expression of Lin-28 during embryonic development in mouse and chicken. *Gene Expression Patterns* 8, 155–160.
- (11) Faas, L., Warrander, F. C., Maguire, R., Ramsbottom, S. A., Quinn, D., Genever, P., and Isaacs, H. V. (2013) Lin28 proteins are required for germ layer specification in *Xenopus*. *Development* 140, 976–986.
- (12) Zhu, H., Shah, S., Shyh-Chang, N., Shinoda, G., Einhorn, W. S., Viswanathan, S. R., Takeuchi, A., Grasmann, C., Rinn, J. L., Lopez, M. F., Hirschhorn, J. N., Palmert, M. R., and Daley, G. Q. (2010) Lin28a transgenic mice manifest size and puberty phenotypes identified in human genetic association studies. *Nat. Genet.* 42, 626–630.
- (13) West, J. A., Viswanathan, S. R., Yabuuchi, A., Cunniff, K., Takeuchi, A., Park, I.-H., Sero, J. E., Zhu, H., Perez-Ayde, A., Frazier, A. L., Surani, M. A., and Daley, G. Q. (2009) A role for Lin28 in primordial germ-cell development and germ-cell malignancy. *Nature* 460, 909–913.
- (14) Zhu, H., Shyh-Chang, N., Segrè, A. V., Shinoda, G., Shah, S. P., Einhorn, W. S., Takeuchi, A., Engreitz, J. M., Hagan, J. P., Kharas, M.

G., Urbach, A., Thornton, J. E., Triboulet, R., Gregory, R. I., Altschuler, D., and Daley, G. Q. (2011) The Lin28/let-7 axis regulates glucose metabolism. *Cell* 147, 81–94.

(15) Viswanathan, S. R., Powers, J. T., Einhorn, W., Hoshida, Y., Ng, T. L., Toffanin, S., O'Sullivan, M., Lu, J., Phillips, L. A., Lockhart, V. L., Shah, S. P., Tanwar, P. S., Mermel, C. H., Beroukhi, R., Azam, M., Teixeira, J., Meyerson, M., Hughes, T. P., Llovet, J. M., Radich, J., Mullighan, C. G., Golub, T. R., Sorensen, P. H., and Daley, G. Q. (2009) Lin28 promotes transformation and is associated with advanced human malignancies. *Nat. Genet.* 41, 843–848.

(16) Yang, X., Lin, X., Zhong, X., Kaur, S., Li, N., Liang, S., Lassus, H., Wang, L., Katsaros, D., Montone, K., Zhao, X., Zhang, Y., Bützow, R., Coukos, G., and Zhang, L. (2010) Double-negative feedback loop between reprogramming factor LIN28 and microRNA let-7 regulates aldehyde dehydrogenase 1-positive cancer stem cells. *Cancer Res.* 70, 9463–9472.

(17) Li, N., Zhong, X., Lin, X., Guo, J., Zou, L., Tanyi, J. L., Shao, Z., Liang, S., Wang, L.-P., Hwang, W.-T., Katsaros, D., Montone, K., Zhao, X., and Zhang, L. (2012) Lin-28 homologue A (LIN28A) promotes cell cycle progression via regulation of cyclin-dependent kinase 2 (CDK2), cyclin D1 (CCND1), and cell division cycle 25 homolog A (CDC25A) expression in cancer. *J. Biol. Chem.* 287, 17386–17397.

(18) Hagan, J. P., Piskounova, E., and Gregory, R. I. (2009) Lin28 recruits the TUTase Zcchc11 to inhibit let-7 maturation in mouse embryonic stem cells. *Nat. Struct. Mol. Biol.* 16, 1021–1025.

(19) Chang, H.-M., Triboulet, R., Thornton, J. E., and Gregory, R. I. (2013) A role for the Perlman syndrome exonuclease Dis3l2 in the Lin28-let-7 pathway. *Nature* 497, 244–248.

(20) Nam, Y., Chen, C., Gregory, R. I., Chou, J. J., and Sliz, P. (2011) Molecular basis for interaction of let-7 microRNAs with Lin28. *Cell* 147, 1080–1091.

(21) Mayr, F., Schütz, A., Döge, N., and Heinemann, U. (2012) The Lin28 cold-shock domain remodels pre-let-7 microRNA. *Nucleic Acids Res.* 40, 7492–7506.

(22) Desjardins, A., Bouvette, J., and Legault, P. (2014) Stepwise assembly of multiple Lin28 proteins on the terminal loop of let-7 miRNA precursors. *Nucleic Acids Res.* 42, 4615–4628.

(23) Desjardins, A., Yang, A., Bouvette, J., Omichinski, J. G., and Legault, P. (2012) Importance of the NCp7-like domain in the recognition of pre-let-7g by the pluripotency factor Lin28. *Nucleic Acids Res.* 40, 1767–1777.

(24) Warrander, F., Faas, L., Kovalevskiy, O., Peters, D., Coles, M., Antson, A. A., Genever, P., and Isaacs, H. V. (2016) Lin28 proteins promote expression of 17 ~ 92 family miRNAs during amphibian development. *Dev. Dyn.* 245, 34–46.

(25) Piskounova, E., Viswanathan, S. R., Janas, M., LaPierre, R. J., Daley, G. Q., Sliz, P., and Gregory, R. I. (2008) Determinants of microRNA processing inhibition by the developmentally regulated RNA-binding protein Lin28. *J. Biol. Chem.* 283, 21310–21314.

(26) Piskounova, E., Polytarchou, C., Thornton, J. E., LaPierre, R. J., Pothoulakis, C., Hagan, J. P., Iliopoulos, D., and Gregory, R. I. (2011) Lin28A and Lin28B inhibit let-7 microRNA biogenesis by distinct mechanisms. *Cell* 147, 1066–1079.

(27) Zuker, M. (2003) Mfold web server for nucleic acid folding and hybridization prediction. *Nucleic Acids Res.* 31, 3406–3415.

(28) Landais, S., Landry, S., Legault, P., and Rassart, E. (2007) Oncogenic Potential of the miR-106–363 Cluster and its implication in human T-cell leukemia. *Cancer Res.* 67, 5699–5707.

(29) He, L., Thomson, J. M., Hemann, M. T., Hernando-Monge, E., Mu, D., Goodson, S., Powers, S., Cordon-Cardo, C., Lowe, S. W., Hannon, G. J., and Hammond, S. M. (2005) A microRNA polycistron as a potential human oncogene. *Nature* 435, 828–833.

(30) Qiao, J., Lee, S., Paul, P., Theiss, L., Tiao, J., Qiao, L., Kong, A., and Chung, D. H. (2013) miR-335 and miR-363 regulation of neuroblastoma tumorigenesis and metastasis. *Surgery* 154, 226–233.

(31) Sun, Q., Zhang, J., Cao, W., Wang, X., Xu, Q., Yan, M., Wu, X., and Chen, W. (2013) Dysregulated miR-363 affects head and neck cancer invasion and metastasis by targeting podoplanin. *Int. J. Biochem. Cell Biol.* 45, 513–520.

(32) Ng, S.-B., Yan, J., Huang, G., Selvarajan, V., Tay, J. L.-S., Lin, B., Bi, C., Tan, J., Kwong, Y.-L., Shimizu, N., Aozasa, K., and Chng, W.-J. (2011) Dysregulated microRNAs affect pathways and targets of biologic relevance in nasal-type natural killer/T-cell lymphoma. *Blood* 118, 4919–4929.

(33) von Hippel, P. H., and Berg, O. G. (1989) Facilitated target location in biological systems. *J. Biol. Chem.* 264, 675–678.

(34) Widom, J. (2005) Target site localization by site-specific, DNA-binding proteins. *Proc. Natl. Acad. Sci. U. S. A.* 102, 16909–16910.

(35) Bonnet, I., Biebricher, A., Porté, P.-L., Loverdo, C., Bénichou, O., Voiturier, R., Escudé, C., Wende, W., Pingoud, A., and Desbiolles, P. (2008) Sliding and jumping of single EcoRV restriction enzymes on non-cognate DNA. *Nucleic Acids Res.* 36, 4118–4127.

(36) Hammar, P., Leroy, P., Mahmutovic, A., Marklund, E. G., Berg, O. G., and Elf, J. (2012) The lac repressor displays facilitated diffusion in living cells. *Science* 336, 1595–1598.

(37) Zeng, Y., Yao, B., Shin, J., Lin, L., Kim, N., Song, Q., Liu, S., Su, Y., Guo, J. U., Huang, L., Wan, J., Wu, H., Qian, J., Cheng, X., Zhu, H., Ming, G.-l., Jin, P., and Song, H. (2016) Lin28A binds active promoters and recruits Tet1 to regulate gene expression. *Mol. Cell* 61, 153–160.

## ■ NOTE ADDED AFTER ASAP PUBLICATION

This article was published ASAP on September 1, 2016, and reposted on September 2, 2016, to correct an error in the spelling of an author's surname.